Paper E

A pore network model for calculation of interfacial velocities*

* Submitted to Advances in Water Resources, fall 2001.

A PORE NETWORK MODEL FOR CALCULATION OF INTERFACIAL VELOCITIES

H.F. Nordhaug [a], M. Celia [b], H.K. Dahle [a]

[a] *Department of Mathematics, University of Bergen, Johs. Brunsgt. 12, N-5008 Bergen, Norway*

[b] *Department of Civil and Environmental Engineering, Princeton University, Princeton, NJ 08544, USA*

Abstract

Two-phase flow in porous media is characterized by fluid-fluid interfaces that separate the fluid phases at the pore scale. These interfaces support pressure differences between phases, and their dynamics allow for saturation changes within the porous medium. Dynamic pore-scale network models allow interface dynamics to be modeled explicitly, such that each fluid-fluid interface within a network of pores is tracked explicitly in space and time. Because these models produce a detailed description of both phase and interface dynamics, results from these models can be averaged to provide values for many upscaled variables. These include nontraditional variables such as amounts of interfacial area, and volume-averaged interfacial velocities. While these upscaled variables provide insights into the underlying dynamics of two-phase flow systems, they also allow new theories involving interfacial area to be tested directly. Results from a test of one such theory reveals that proposed constitutive equations involving interfacial velocities fail to match results from the network model for most cases considered. Therefore the macroscopic equations require additional development before they can be used for macro-scale simulations.

Key words: Two-phase flow, dynamic pore-scale network models, interfacial area, upscaling

1 Introduction

Multi-phase porous media systems are characterised by fluid-fluid interfaces that exist at the pore scale. These interfaces define the spatial boundaries of each phase

Email addresses: hansfn@mi.uib.no (H.F. Nordhaug), celia@princeton.edu (M. Celia), reshd@mi.uib.no (H.K. Dahle).

at any given instant in time. Interfaces also have properties such as interfacial tension, which allows each fluid to maintain a different pressure. The resulting difference between individual phase pressures is usually called capillary pressure. Fluid-fluid interfaces also provide the surfaces across which mass is transferred from one fluid phase to another, in problems such as dissolution of non aqueous phase liquid (NAPL) into flowing ground waters. Fluid-solid interfaces provide similar surfaces for mass exchanges between fluid and solid phases. For these reasons, an understanding of interfacial behaviour at the pore scale, and subsequent scaling of that behaviour to the more practical continuum scale, is important to proper descriptions of porous media flow systems.

The view that interfacial area plays an important role in porous media flows is supported by the recent theoretical developments reported by Gray and Hassanizadeh [1]. In their remarkable work, a thermodynamic approach is used to show that the relationship between capillary pressure and saturation is incomplete, and that specific interfacial area (defined as amount of interfacial area per unit volume of porous medium) should enter into the relationship. Therefore one should seek a relationship between capillary pressure, saturation, and interfacial area(s). Such a relationship has been derived, using a pore-scale network model, by Reeves and Celia [2]. Other simulation studies have explored a variety of additional aspects of the new theories of Gray and Hassanizadeh, see for example Held and Celia [3]. One of the intriguing aspects of the theoretical developments of Gray and Hassanizadeh is the inclusion of equations based on interface dynamics. That is, in order to properly account for interfacial effects in the governing equations, new equations must be written to take account of interfacial dynamics. These are based on conservation laws written for the interfaces, with associated constitutive relations.

One of the difficulties associated with tests of theories involving interfacial areas is the lack of experimental procedures to measure these areas. While partitioning tracers offer hope for inferring amounts of area (for example Heonki et al. [4]), and novel laboratory procedures and equipment offer hope for more direct measurement of interfacial areas (Montemagno and Gray [5]), experimental determination of interfacial area is still a daunting task. And experimental determination of interfacial dynamics, which tends to occur on very short time scales, is even more difficult. Therefore, testing of these theories must rely on use of specific kinds of computational models, including so-called pore-scale network models. Pore-scale network models typically represent the pore space of the medium using simplified geometries, and within this geometric representation solve equations to track explicitly the location of all fluid-fluid interfaces within the network. Typical geometric representations include regular lattice structures, such as a cubic lattice, with pore bodies corresponding to the vertices of the lattice, and pore throats connecting the pore bodies. Pore bodies are often assigned spherical shapes, although cubes or other shapes with corners are sometimes used to account for wedge and corner flows. Similarly, pore throats may be cylindrical with circular cross section, or cylindrical with rectangular or perhaps triangular cross sections. For all of these choices, the

geometry is kept sufficiently simple that interface configurations can be calculated analytically, for a given set of fluid pressures. These models are often run to mimic typical laboratory experiments, such as pressure cell tests to determine the relationship between capillary pressure and relative fluid saturation. This is accomplished by use of lattices that are sufficiently large to define meaningful continuum-scale measures, such as fluid saturation. Results of such simulations show all of the major features of experimental relationships, including finite entry pressures, residual saturations, and hysteresis. Because the simulators define interface geometries explicitly, additional geometric information may be extracted from network models. For example, fluid-fluid interfacial area can be calculated easily, given knowledge about the location and shape of each fluid-fluid interface.

Two general types of pore-scale network models may be identified: quasi-static models and dynamic models. In a quasi-static models, the location of any fluid-fluid interface is governed by equilibrium considerations only. Equilibrium states are determined from the Young-Laplace equation, which relates the capillary pressure to the interfacial tension and the interface curvature, viz. (Dullien [6])

$$P_c = \frac{\sigma}{R} \tag{1}$$

In this equation, σ is interfacial tension and R is the radius of curvature. Depending on the shapes chosen for the pore elements, the Young-Laplace equation is modified to include contact angles and pore geometry to develop rules about whether or not an interface is stable at a given location, given an imposed capillary pressure. If the interface is unstable, it is moved through the network until a stable position is found, or until it exits the network. No time dependence is included in the calculation; the interface is simply moved from one equilibrium position to another. This type of model is consistent with an algebraic relationship between capillary pressure and saturation, where changes in capillary pressure are translated instantaneously to changes in saturation. Examples of these kinds of models include those described by Dullien [6], Ferrand and Celia [7], and Reeves [8], among many others.

A second type of pore network model involves computation of transient behaviour associated with interface movement. That is, unstable interfaces are tracked through the network until a stable position is reached, but the transient nature of the movement from one position to another is explicitly described and modeled. While these transient models are more computationally complex, they allow the underlying transients associated with interface movement to be incorporated and analysed explicitly. While most pore-scale network models reported in the literature are quasi-static, there have been several dynamic models that have been developed. These include the model of Blunt and King [9]; a series of models by Payatakes and coworkers (see, for example, Valavanides and Payatakes [10]), and more recent models by Mogensen and Stenby [11], Aker et al. [12], Hassanizadeh (Dijkstra et al. [13]) and by Dahle and Celia [14]. The models of Payatakes are the most

comprehensive, including a focus on mobilization of trapped fluids and so-called drop traffic flows.

In this paper, we use a model based on the original work of Blunt and King [9] and calculate dynamic interfacial behaviour, with focus on volume-averaged interfacial velocity. After describing the salient features of the model, and providing a definition of average interfacial velocity, specific calculations are performed to demonstrate how continuum-scale measures of both interface velocity and phase velocity can be quantified. The model is then used to test a specific theoretical conjecture regarding interfacial velocity and its relationship to average phase velocities. We show fundamental differences between stable and unstable displacements, and discuss how these differences impact the comparisons between theory and model results.

2 The dynamic network model

The pore-scale network model used herein is an extension of the model of Blunt and King [9]. The pore network is a rectangular lattice, with spherical pore bodies and cylindrical pore throats, with pore-size distributions defined for the bodies and throats, see Figure 1(a). Following Blunt and King [9], the model is simplified by the following assumptions: (1) local capillary pressure in the pore throats is assumed to be negligible, so that only one pressure exists within a pore body, independent of the local saturation of that pore body; (2) while the radius of a pore throat, r_{ij}, serves to define its hydraulic conductance, the volume contributed by the pore throat is assumed to be small relative to volumes of pore bodies, therefore movement of an interface through a pore throat is assumed to occur instantaneously; (3) flow within pore throats is assumed to be laminar and given by Poiseuille's law; (4) both fluids are assumed to be incompressible. With these assumptions, the set of governing equations is relatively simple. Each equation must obey volume conservation within each pore body, such that

$$V_i \frac{dS_i^\alpha}{dt} + \sum_{j \in N_i} Q_{ij}^\alpha = 0 \tag{2}$$

where V_i represents the volume of pore body i, S^α represents local saturation (percent of V_i filled with fluid α), Q_{ij}^α is the volumetric flux from pore body i to it's neighbour j, and N_i is a list of all neighbour pore bodies for pore body i. This equation is written for both fluid phases, wetting ($\alpha = w$) and non-wetting ($\alpha = n$). The volumetric flux is related to pressures at the pore bodies by Poiseuille's law,

$$Q_{ij}^\alpha = G_{ij}^\alpha (p_i^\alpha - p_j^\alpha) \tag{3}$$

where p_l^α represents pressures, and G_{ij}^α represents hydraulic conductance in the pore throat connecting pore bodies i and j. Because the pore throats are cylindrical, and interface movement through them is instantaneous, only one fluid can occupy a given pore throat, at a given time. Therefore the fluid occupying the pore throat has conductance

$$G_{ij}^\alpha = \frac{\pi r_{ij}^4}{8\mu^\alpha l_{ij}}, \tag{4}$$

while the non-occupying fluid has zero conductance. Summation of Equation (2) over the two phases gives the equation

$$\sum_{j \in N_i} (Q_{ij}^w + Q_{ij}^n) = 0 \tag{5}$$

Substitution of Equation (3) for each of the phase fluxes Q_{ij}^α provides a set of algebraic equations with the pore-body pressures as unknowns. These can be solved using standard matrix solution methods.

In the simulations reported herein, we only consider drainage, so that the resident fluid is the wetting fluid, and the invading fluid is non-wetting fluid. Time steps are chosen so that during any time step, only one pore body reaches full non-wetting phase saturation. That pore body then generates additional interfaces, located at all connecting pore throats that are filled with wetting fluid. Those interfaces are then tested for capillary stability, using the most recent pore body pressures. If they are stable, they remain in place, and the connecting pore throat is marked as trapped, with conductances set to zero for both phases. If the interface is unstable, it passes through the pore throat, non-wetting fluid occupies the pore throat, and non-wetting fluid can then begin to invade the adjoining pore body.

Overall, the algorithm proceeds as an Implicit Pressure Explicit Saturation (IMPES) routine. The major unknowns are the pressure and saturation of each pore body. For a given distribution of fluids, phase conductances are calculated and put into Equation (5), which is solved for a new pressure field. That pressure field is then used in Equation (3) to compute fluxes through the pore throats. These fluxes are then used, in conjunction with knowledge of the current saturations in each pore body, to determine the minimum filling time for each of the pores, and this is set as the time step size. Then Equation (2) is used to update the saturations in each pore body. Newly created interfaces are tested for stability, conductances are updated, and the procedure is repeated. In the matrix solution for pressures, regions of wetting fluid that become completely surrounded by non-wetting fluid, and are therefore hydraulically trapped, are removed from the matrix equations to avoid singular matrices. This algorithm provides a transient response for both pressure and saturation.

This overall leads naturally to investigations of relationships between these variables, as well as others, such as interfacial area. In order to calculate these variables,

averages need to be defined over a representative volume. The volume might be chosen to correspond to the entire volume of the network, or it might be defined as essentially two-dimensional slices through the network, in the direction perpendicular to the macroscopic direction of displacement. In either case, volume-averaged saturation is defined as

$$S^{\alpha} = \frac{\sum_{i \in N_{vol}} V_i S_i^{\alpha}}{\sum_{i \in N_{vol}} V_i} = \frac{1}{V} \sum_{i \in N_{vol}} V_i S_i^{\alpha} \tag{6}$$

where V is the volume of the chosen averaging region, and N_{vol} denotes the set of pore bodies within the chosen averaging volume. Capillary pressure is defined as the difference between volume-averaged phase pressures, such that

$$P_c = p_n - p_w = \frac{1}{V}\Big(\sum_{i \in N_{vol}} V_i S_i^n p_i - \sum_{i \in N_{vol}} V_i S_i^w p_i \Big) \tag{7}$$

where p_i corresponds to the pressure in pore body i. Notice that while no local capillary pressure exists (by assumption in the model), a macroscopic capillary pressure is still well defined based on the average phase pressures.

Average properties associated with interfaces require somewhat more care in their definitions. Because no capillary pressure is associated with individual pore bodies, the shape (especially the curvature) of a particular interface is not specified. The only information for active (non-trapped) interfaces is that they reside in a specific pore body. To assign a measure of interfacial area, an interface within a filling pore body is assigned an area equal to the diameter of the pore body. Those interfaces trapped at the entrance to pore throats are assigned the area associated with the diameter of the pore throat. Therefore, the specific interfacial area, defined as the amount of interfacial area per unit volume of porous medium, is defined as

$$a^{wn} = \frac{1}{V}\Big(\sum_{i \in N_{vol}} a_i^{wn} + \sum_{j \in M_{vol}} a_j^{wn} \Big) = \frac{A^{wn}}{V} \tag{8}$$

where M_{vol} denotes the set of pore throats that are contained within the averaging volume V.

The averaged variable that is the most difficult to define is the volume-averaged interfacial velocity. Because interfaces that reside within pore bodies are not resolved, their velocities need to be inferred from fluxes into and out of the pore body, changes in saturation within the pore body, and lengths of travel associated with the pore body and its connected pore throats. Consider a fluid-fluid interface that is spawned by complete filling of a given pore body. It first comes into contact with the connected pore throat, and a capillary stability test is performed. If the interface experiences sufficient capillary pressure to drive it through the pore throat, it will move through the throat with infinite velocity, then will fill the connected

pore body at some finite rate, given by the subsequent computed changes in saturation for that pore body. The infinite speed is a consequence of the simplifying assumption that the pore throats are volumeless. To define a finite speed that preserves proper global velocities, the pore filling associated with saturation changes is extended in length to cover the combined pore body – pore throat combination, and the 'locally averaged' velocity for a specific interface is defined as

$$\|\mathbf{v}_i^{wn}\| = l_{i,j}\frac{\Delta S_i^n}{\Delta t} \tag{9}$$

where the double brackets signify magnitude of the interface velocity vector, the length $l_{i,j}$ denotes the length of the pore throat through which the entering interface travels plus the diameter of the pore body i, and ΔS_i^n denotes the change in saturation over the time interval Δt. The direction assigned to the interfacial velocity vector is the average of the total inflow vector and total outflow vector. Finally, the volume-averaged velocity vector is given by the sum of each interfacial velocity weighted by the area of the interface,

$$\mathbf{v}^{wn} = \frac{1}{A^{wn}}\sum_{i\in N_{vol}} \mathbf{v}_i^{wn} a_i^{wn} \tag{10}$$

Volume-averaged phase velocities may be defined analogously to average interfacial velocities with volume replacing areas as the appropriate weights, such that

$$\mathbf{v}^{\alpha} = \frac{1}{V S^{\alpha}}\sum_{i\in N_{vol}} \mathbf{v}_i^{\alpha} V_i S_i^{\alpha} \tag{11}$$

where $\mathbf{v}_i^{\alpha}$ is given by an equation similar to Equation (9), with appropriate modification for the case of $S = 1$ or $S = 0$.

3 Theoretical Conjectures

One of the more intriguing developments in the past decade has been proposal of a new set of governing equations for two-phase flow in porous media. These equations include volume-averaged, specific interfacial area as a key variable. Among other things, capillary pressure and saturation must have an extended relationship that includes interfacial area; conservation equations are written for interfaces, and these equations include interfacial area as a dependent variable; and new constitutive relationships proposed to close this expanded equation set include interfacial area as a key component. Examples of these equations include the following:

$$\frac{da^{wn}}{dt} + \nabla\cdot(\mathbf{G}^{wn} a^{wn} \mathbf{v}^{wn}) = F^{wn} \tag{12}$$

where $\mathbf{G}^{wn}$ is a geometric tensor and F^{wn} refers to a general production term for interfacial area (see [15]). Also, as a proposed constitutive relationship for interfacial velocities, Nordhaug et al. [15] have proposed the following relationship between volume-averaged interface velocity and volume-averaged phase velocities:

$$(\mathbf{R}^{w}_{wn} + \mathbf{R}^{n}_{wn}) \cdot \mathbf{v}^{wn} = \mathbf{R}^{w}_{wn} \cdot \mathbf{v}^{w} + \mathbf{R}^{n}_{wn}\mathbf{v}^{n} \tag{13}$$

In this equation, the coefficients $\mathbf{R}^{\alpha}_{wn}$ represent resistances to flow, and could be functions of phase saturation(s) or other variables. The general idea of the equation is that the interfacial velocity should be a weighted sum of the phase velocities. While the resistance coefficients may be unknown, the general concept can be tested via the network model. Similarly, the terms in the earlier equation (Equation (12)) can be determined from the network model, and therefore the equation may be tested for validity. Because these variables cannot be measured experimentally at this time, the only tool available to test these proposed new equations is the network simulator. This is how we use the network model in the next section, as continuum-scale variables are computed and the equations proposed above are evaluated and tested.

3.1 Modeling of resistance terms $\mathbf{R}^{\alpha}_{wn}$

In [15] a complete model for two phase flow including interfacial area was presented. We provide a few of the key equations to illustrate the ideas. The governing equations includes Equation (12) and (13) which are geometric constraint and momentum balance equations, respectively, written for a massless interface. In addition, phase equations for mass and momentum written as:

$$\frac{\partial(\varepsilon^{\alpha}\rho^{\alpha})}{\partial t} + \varepsilon^{\alpha}\rho^{\alpha}\nabla \cdot \mathbf{v}^{\alpha} = 0. \tag{14}$$

and

$$-\varepsilon^{\alpha}\nabla p^{\alpha} + \varepsilon^{\alpha}\rho^{\alpha}\mathbf{v} = (\mathbf{R}^{\alpha}_{wn} + \mathbf{R}^{\alpha}_{\alpha s}) \cdot \mathbf{v}^{\alpha} - \mathbf{R}^{\alpha}_{wn} \cdot \mathbf{v}^{wn}. \tag{15}$$

The functionality of the resistance terms $\mathbf{R}^{\alpha}_{wn}$ and $\mathbf{R}^{\alpha}_{\alpha s}$ in Equation (13) and (15) were assumed to be as follows:

$$\begin{aligned}
\mathbf{R}^{w}_{wn} &= \mu^{w} g^{w}_{wn}(a^{wn}) h^{w}_{wn}(s^{w}) \mathbf{K}^{-1} {\varepsilon^{w}}^{2}, \\
\mathbf{R}^{w}_{ws} &= \mu^{w} g^{w}_{ws}(a^{ws}) h_{w}(s^{w}) \mathbf{K}^{-1} {\varepsilon^{w}}^{2}, \\
\mathbf{R}^{n}_{wn} &= \mu^{n} g^{n}_{wn}(a^{wn}) h^{n}_{wn}(s^{n}) \mathbf{K}^{-1} {\varepsilon^{n}}^{2}, \\
\mathbf{R}^{n}_{ns} &= \mu^{n} g^{n}_{ns}(a^{ns}) h_{n}(s^{n}) \mathbf{K}^{-1} {\varepsilon^{n}}^{2}.
\end{aligned}$$

These functional forms were chosen according to the following observations in [15]. Equation (15) is a generalised form of Darcy's law. When the saturation goes

to zero or one for one of the phases Equation (15) should reduce to the normal Darcy's law for two phase flow. The viscosity and permeability terms, μ^α and $\mathbf{K}$, are included to make the dimensions match on the left and right hand sides. The g's and h's must be non-dimensional (and positive). The volume fraction terms, ${\epsilon^\alpha}^2$, are added to be able to go from average phase velocities to Darcy velocities.

By considering the results from the network model we should be able to investigate whether Equation (13) is reasonable. However, to be able to say something quantitative about the resistance terms $\mathbf{R}^\alpha_{wn}$ we must use the definitions above. When $\mathbf{K}$ is a scalar we get the following expression for the interface velocity [15]:

$$\mathbf{v}^{wn} = F^w\mathbf{v}^w + F^n\mathbf{v}^n = \frac{f^w}{f^w + f^n}\mathbf{v}^w + \frac{f^n}{f^w + f^n}\mathbf{v}^n \tag{16}$$

where we have chosen

$$f^\alpha = (1 - s^\alpha)^3(s^\alpha)^2. \tag{17}$$

4 Equation testing and numerical results

In the following we use a three-dimensional pore network to compute averaged interfacial and phase velocities. We use these computed velocities to test the theoretical conjecture given in Equation (13). We also compute other averaged variables, such as specific interfacial area, to demonstrate certain behavior patterns in the two-phase flow system. For the averaged quantities, we sometimes use a single averaging volume, spanning the entire network, and we sometimes use a 'sliding average' that involves subsets of the total network volume. The latter averaging allows us to compute spatially varying averaged quantities.

4.1 Experimental setup

All simulations are performed on a three-dimensional network of size $10 \times 10 \times 50$ pore bodies. When sliding averages are calculated, the size of the sub-volumes is $10 \times 10 \times 10$, and the averages as calculated along the largest direction (that is, the direction with 50 pore bodies, assumed to be the vertical direction).

Boundary and initial conditions are set up to correspond to primary drainage. The top boundary is set to have a pressure of 4000 Pa, and fixed saturation of $S^w = 0$, while the bottom boundary is set with pressure of 0 Pa and saturation $S^w = 1$. No-flow conditions are imposed along the lateral sides of the domain. The initial condition is taken as $S^w = 1$, with a uniform pressure of 2000 Pa.

Fluid viscosities are chosen so that both stable and unstable displacements are simulated. Table 1 lists the viscosities used for the wetting and nonwetting fluids. While we have performed simulations over a range of viscosity values, we will use three representative values of viscosities so that the viscosity ratio between nonwetting and wetting fluids is 10, 1, and 0.1. In all simulations, the fluids are assigned an interfacial tension of 0.72 [N/m], and the contact angle is set at zero. We ignore density differences between the two fluids.

Table 1
Wetting and non-wetting fluid viscosities

Set	μ_w	μ_{nw}	
1	0.001	0.010	[Ns/m^2]
2	0.001	0.001	[Ns/m^2]
3	0.001	0.0001	[Ns/m^2]

The radii of the pore bodies and pore throats are generated using a cut-off log-normal distribution. The same standard deviation (or the parent distribution) is used for both the bodies and the throats, but different means and upper and lower cut-off values are used. Appropriate information is provided in Table 2.

Table 2
Distribution parameters for pore and throat radius.

	Set 1	
Standard deviation	0.25	
Pore body mean	$1.2 \cdot 10^{-3}$	[m]
Pore body lower cut-off	$0.6 \cdot 10^{-3}$	[m]
Pore body upper cut-off	$1.8 \cdot 10^{-3}$	[m]
Pore throat mean	$4.0 \cdot 10^{-4}$	[m]
Pore throat lower cut-off	$2.0 \cdot 10^{-4}$	[m]
Pore throat upper cut-off	$6.0 \cdot 10^{-4}$	[m]

4.2 Calculation of Local and Averaged Quantities

Numerical solution of the network equations provides values for fluid pressures and associated saturations in each pore body, for each time step. From these values, and the geometry of both the network and the chosen averaging volumes, we compute averaged quantities as post-processing calculations. Because we have information about location and state of all fluid-fluid interfaces, we can distinguish between trapped and moving interfaces. Therefore, when defining averaged quantities, we

may choose to distinguish between averages that include all interfaces, and averages that only involve active interfaces. As the default, we include all interfaces in the calculations, consistent with definitions such as that given in Equation (8). However, there are times when it is useful to isolate only those interfaces that are moving. When averages are taken over active interfaces only, then we focus the calculations on pore bodies only, and we neglect pore throats, including pore throat volumes. The reason is that interfaces that are trapped will reside at the entrance to pore throats, so for consistency between interfacial discrimination and volume calculations, we decided to eliminate pore throat volumes and areas when we ignore trapped interfaces.

4.3 Stable displacement

Several simulations were run with viscosity rations greater than one. To illustrate the case of stable displacement, a viscosity ratio of 10 is used, with the boundary and initial conditions presented above. Network occupancy of fluids is shown in Figure 1(a), for an intermediate time corresponding to movement through the upper portion of the network. A flat, piston-like front can be seen moving through the network. Very little wetting fluid is left behind, with virtually all trapped wetting fluid existing as trapped singlets in pore throats. In Figure 1(b), average saturation, based on the sliding average concept, is plotted as a function of depth. The macroscopic frontal behavior of the displacement is clear in this figure.

Average phase and interfaces velocities may be calculated for this case. In Figure 2, the averaged interfacial velocity is compared to that predicted by Equation (13). The results in Figure 2(a) show that the average interfacial velocity is consistently below the predicted values based on the average phase velocities (Equation (13)). A relatively poor prediction is also seen in the sliding averages shown in Figure 2(b). However, if we exclude the trapped interfaces, and only use active interfaces in the calculations, we find that the theory matches the numerical values quite well, see Figure 3. This is because elimination of trapped interfaces leaves only pores that are actively filling, and the macroscopically flat front means that interfaces are constrained to move with the same velocity of the invading and defending fluids, just as would happen in a single tube or pipe. So viscous stability, which produces flat front macroscopically, lead to active interface velocities that are essentially identical to the two phase velocities, which themselves are equal. In this case, the theoretical equation appears to hold. However, inclusion of all interfaces leads to disparity between the values, due to the presence of trapped interfaces.

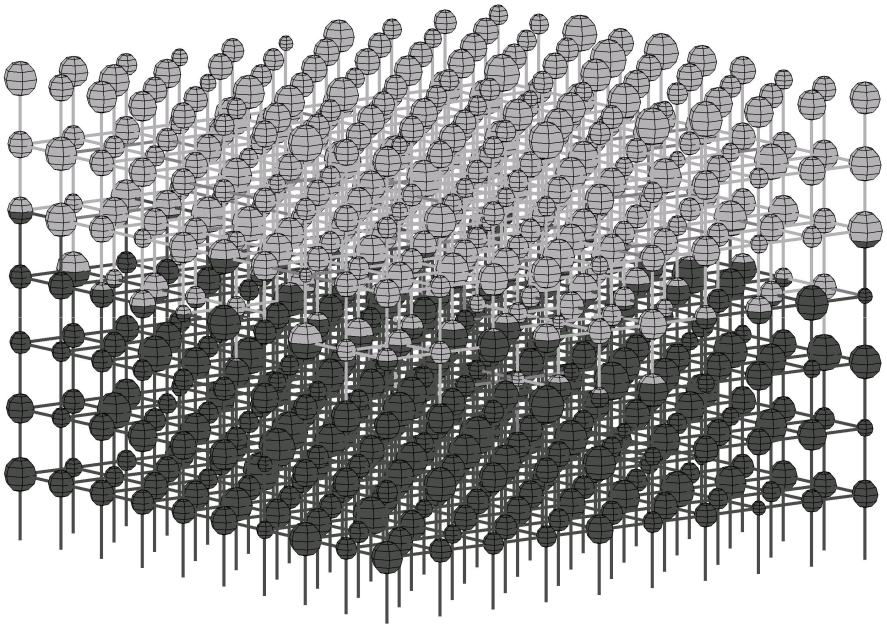

(a) microscale

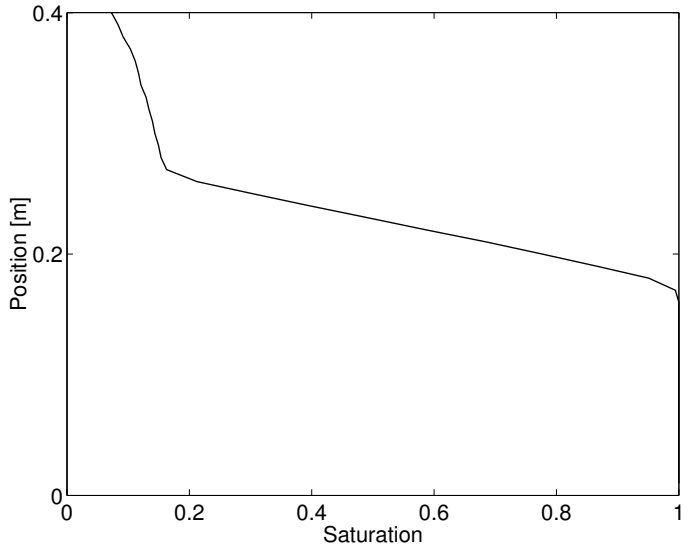

(b) macroscale

Fig. 1. Stable displacement – $M_\mu = 10.0$. Snapshot of the saturation front.

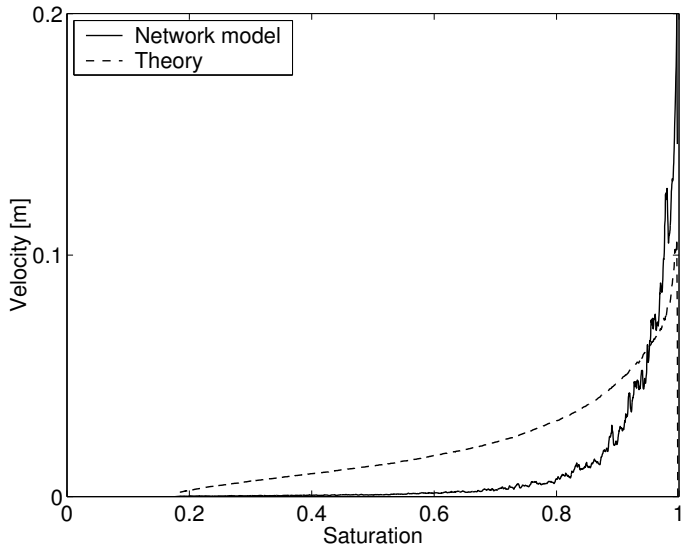

(a)

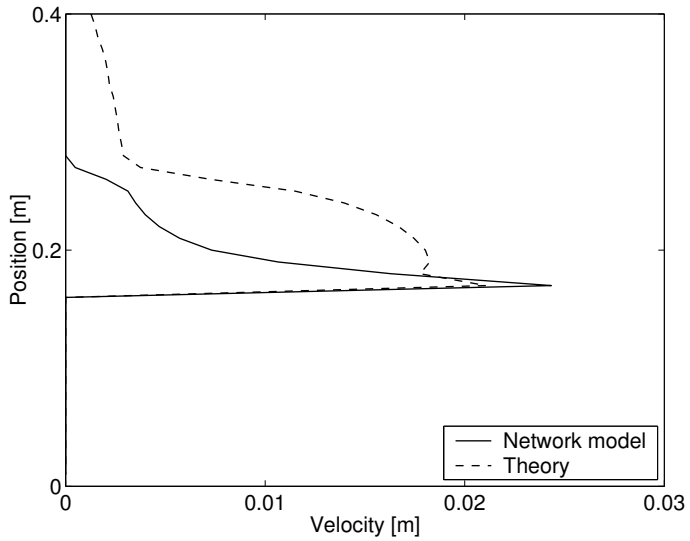

(b)

Fig. 2. Stable displacement – $M_\mu = 10.0$. Comparison of interface velocity in the network model and computed using phase velocities for one REV (a) and sliding REVs (b).

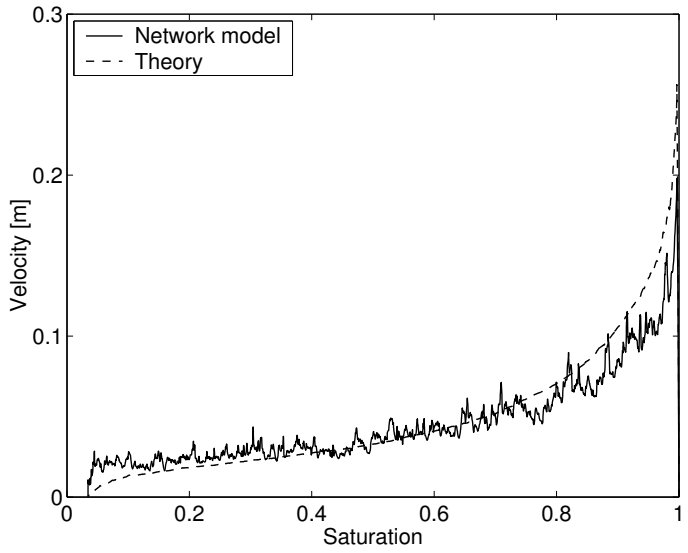

(a)

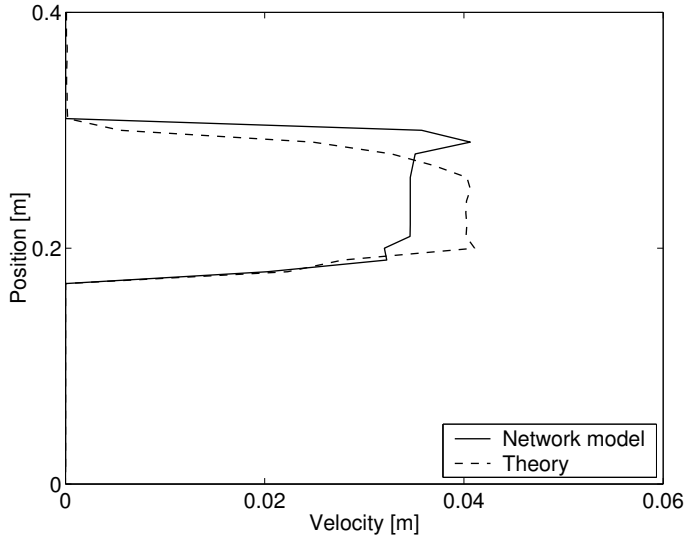

(b)

Fig. 3. Stable displacement – $M_\mu = 10.0$. Comparison of interface velocity in the network model and computed using phase velocities for one REV (a) and sliding REVs (b). Throat volume and trapped interfaces are not acounted for.

4.4 Unstable displacement

To illustrate the model behavior in the case of unstable displacements, we use a viscosity ratio of 0.1, with the same boundary and initial conditions described above. In this case, we expect a much more irregular front, with possible viscous fingering, and this is essentially what we observe. In Figure 4(a), an irregular and fingered pattern is clear from the fluid occupancy plot of the network. The associated sliding average plot showing average saturation as a function of depth (Figure 4(b)) shows a much more dispersed saturation distribution. Now when the average velocities are calculated, there is a very large disparity between average interfacial velocities and average phase velocities. This results in a poor match between the interfacial velocities predicted by Equation (13) and those calculated in the network model. We observe that in the unstable case, local horizontal flows are more prevalent than in the stable case, due to the highly irregular shape of the invading front. However, the dominant flow direction remains the vertical.

To illustrate some additional difference between the stable and unstable displacements, we have plotted amount of interfacial area as a function of saturation for the viscosity ratios of 10, 1, and 0.1. Figure 6(a) shows the amount of trapped interfacial area as a function of saturation, with the most irregular fronts (viscosity ratio of 0.1) producing the largest amount of trapped interfacial area, and the most stable flat front (viscosity ratio of 10) producing the least amount of trapping. The clear trend is for increasing amounts of trapped interfacial area with decreasing viscosity ratio. In Figure 6(b), the amount of active interfacial area is plotted as a function of saturation, again for the three different viscosity ratios. Here we see a more complex relationship, but the unstable displacements clearly produce the largest amount of active interfacial area, but also produces the highest residual wetting phase saturation. The trend moves consistently to lower amounts of active interfacial area, and lower residual saturations, as viscosity ratio increases.

5 Summary and conclusions

The dynamic network model presented herein is relatively simple to implement, and leads to numerical calculations that are straight-forward to implement. The calculation of averages allows many continuum-scale variables to be calculated, and thereby facilitates testing of new theories that involve non-traditional variables. In this work, we have focused on interfacial dynamics, and calculation of average interfacial velocities. We have used these results to test a specific conjecture that relates average interfacial velocity to average phase velocities.

Overall, we conclude that the proposed equation that relates interfacial velocity to phase velocities only hold under very specific conditions, namely piston-like sta-

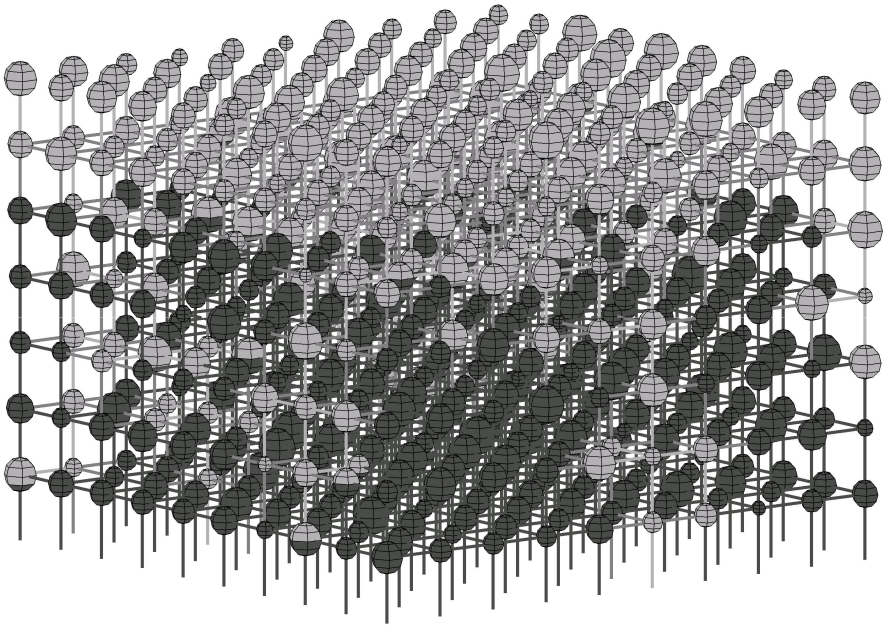

(a) microscale

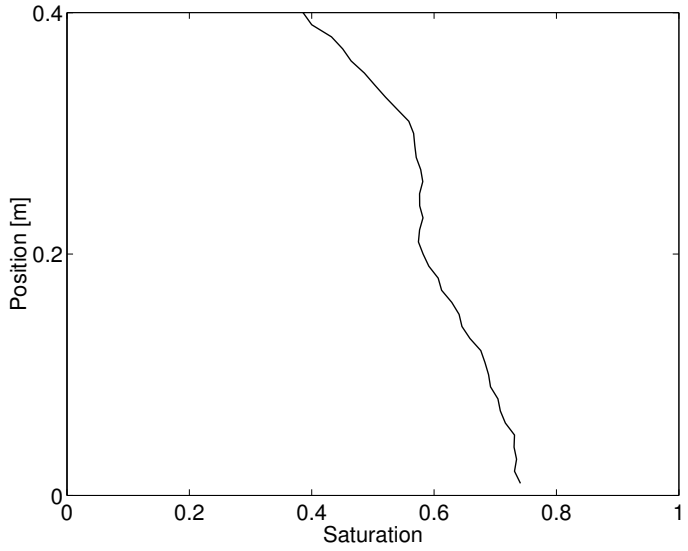

(b) macroscale

Fig. 4. Unstable displacement – $M_\mu = 0.1$. Snapshot of the saturation front.

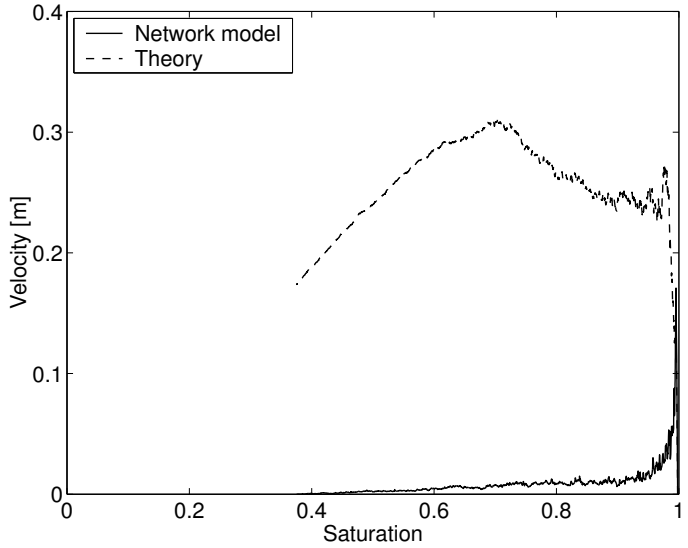

(a)

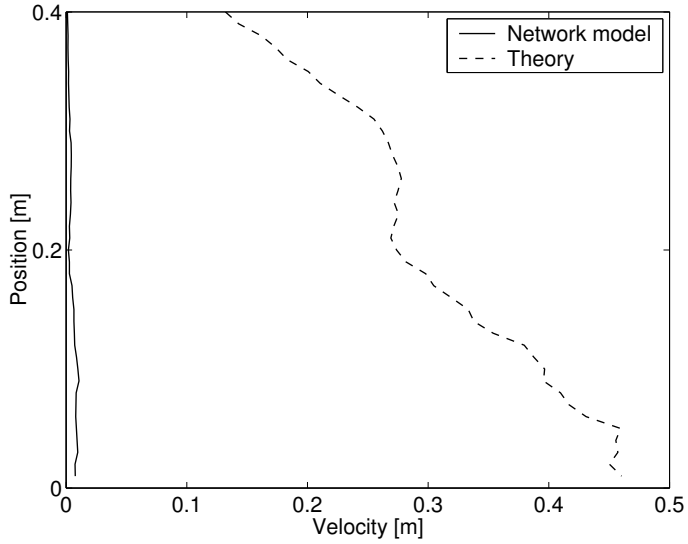

(b)

Fig. 5. Unstable displacement – $M_\mu = 0.1$. Comparison of interface velocity in the network model and computed using phase velocities for one REV (a) and sliding REVs (b).

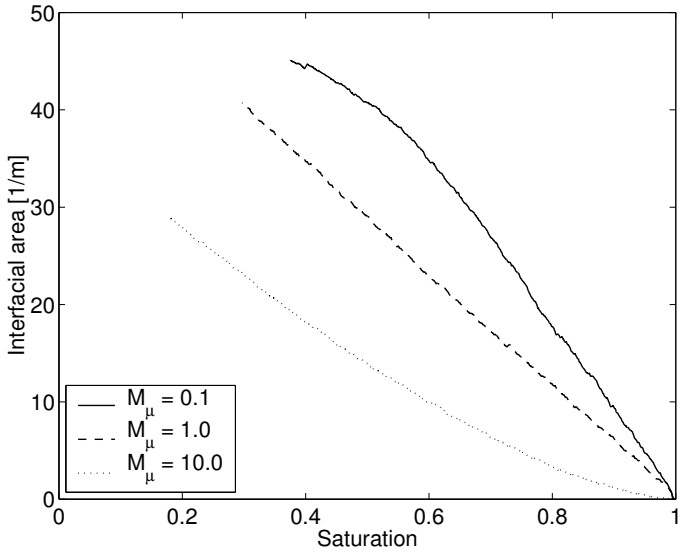

(a) trapped

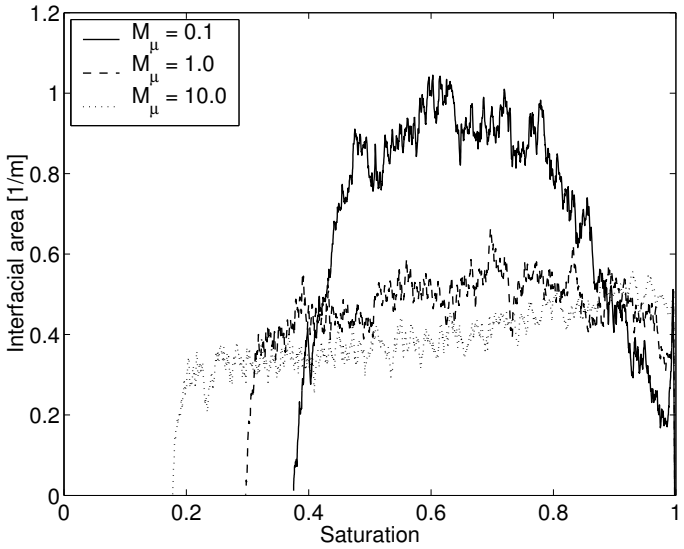

(b) moving

Fig. 6. Amount of interfacial area for different viscosity ratios M_μ.

ble displacements in which trapped interfaces are neglected. Under more general conditions, where the invading front is more irregular and piston displacement does not occur at the macroscopic scale, the equation provides a poor prediction. Therefore new constitutive equations to close the extended set of equations for two-phase flow, which include specific interfacial area as a primary variable, need to be developed.

While this work focused on a specific constitutive equation, the general approach is illustrative of the kinds of problems that can be solved with dynamic pore-scale network models. Such models allow local-scale information to be used directly to define averaged, or upscaled, variables. Because the local-scale information is highly detailed, many upscaled variables can be calculated, including nontraditional ones like interfacial area and average interfacial velocity. This greatly facilitates testing of new theories, and has the potential to provide significantly improved insights into fundamental behaviors in two-phase porous media flows.

Acknowledgements

The authors gratefully acknowledge the contributions of W.G. Gray and S.M. Hassanizadeh to this work. Partial support for this work was provided to M.Celia by the National Science Foundation under Grant EAR-9805376 and to H.F. Nordhaug by the Norwegian Research Council (NFR) under grant 116153/431.

References

[1] W. Gray, S. Hassanizadeh, Macroscale continuum mechanics for multiphase porous-media flow including phases, interfaces, common lines and common points, Advances in Water Resources 21 (4) (1998) 261–281.

[2] P. Reeves, M. Celia, A functional relationship between capillary pressure, saturation, and interfacial area as revealed by a pore-scale network model, Water Resources Research 32 (8) (1996) 2345–2358.

[3] R. Held, M. Celia, Modeling support of functional relationships between capillary pressure, saturation, interfacial area, and common lines, Advances in Water Resources 24 (3-4) (2001) 325–343.

[4] K. Heonki, P. Rao, M. Annable, Determination of effective air-water interfacial area in partially saturated porous media using surfactant adsorption, Water Resources Research 33 (12) (1997) 2705–2711.

[5] C. Montemagno, W. Gray, "photoluminescent volumetric imaging: A technique for the exploration of multiphase flow and transport in porous media, Geophysical Research Letters 22 (4) (1995) 425–428.

[6] F. Dullien, Porous Media: Fluid Transport and Pore Structure, 2nd Edition, Academic Press, 1992.

[7] L. Ferrand, M. Celia, The effect of heterogeneity on the drainage capillary pressure - saturation relation, Water Resources Research 28 (3) (1992) 859–870.

[8] P. Reeves, The development of pore-scale network models for the simulation of capillary pressure - saturation - interfacial area - relative permeability relationships in multi-fluid porous media, Ph.D. thesis, Department of Civil Engineering and Operations Research, Princeton University (1997).

[9] M. Blunt, P. King, Relative permeabilities from 2-dimensional and 3-dimensional pore-scale network modeling, Transport in porous media 6 (4) (1991) 407–433.

[10] M. Valavanides, A. Payatakes, True-to-mechanism model of steady-state two-phase flow in porous media, using decomposition into prototype flows, Advances in Water Resources 24 (3-4) (2001) 385–407.

[11] K. Mogensen, E. Stenby, A dynamic two-phase pore-scale model for imbibition, Transport in Porous Media 32 (1998) 299–327.

[12] E. Aker, K. Maloy, A. Hansen, G. Batrouni, A two-dimensional network simulator for two-phase flow in porous media, Transport in Porous Media 32 (1998) 163–186.

[13] T. Dijkstra, G. Bartelds, J. Bruining, S. Hassanizadeh, Dynamic pore-scale network for two-phase flow, in: van Genuchten et al. (Ed.), Characterization and Measurement of the Hydraulic Properties of Unsaturated Soils, 1999, pp. 63–69.

[14] H. Dahle, M. Celia, A dynamic network model for two-phase immiscible flow, Computational Geosciences 3 (1999) 1–22.

[15] H. Nordhaug, H. Dahle, M. Espedal, W. Gray, M. Celia, Two phase flow including interfacial area as a variable, in: L. Bentley, J. Sykes, C. Brebbia, W. gray, P. G.F (Eds.), Computational Methods in Water Resources, Vol. 1, A.A Balkema, 2000, pp. 231–238.